Dalton Transactions

Accepted Manuscript

ROYAL SOCIETY OF CHEMISTRY

www.rsc.org/dalton

Dalton Transactions

Manuscript ID: DT-ART-01-2014-000265.R1

Role of structural and fluidic aspects of Room temperature ionic liquid in influencing the morphology of CdSe nano/microstructures grown *in situ*

Apurav Guleria, Ajay K. Singh, Madhab C. Rath, Sisir K. Sarkar and Soumyakanti Adhikari*

Radiation & Photochemistry Division, Bhabha Atomic Research Centre, Mumbai 400 085, India

Abstract

RTILs as a media to synthesize variety of nanomaterials are gaining momentum owing to their unique physicochemical properties. However, the fundamental questions regarding the role of the inherent structure of IL in directing the morphology and the growth mechanism of the nanoparticles are still unexplored. Therefore, an attempt was made in this respect wherein CdSe nanoparticles were synthesized in *neat* room temperature ionic liquid (RTIL), 1-ethyl-3-methyl imidazolium ethylsulfate ([EMIM][$EtSO_4$]) at ambient conditions. The IL was found to play three roles, as a solvent, as stabilizing agent and as a shape directing template. The primary nanoparticles were of the sizes in the range of 2-5 nm, as determined by the HR-TEM. These primary nanoparticles grow into nanoflake like units which further self-assemble and transform into a mixture of anisotropic nanostructures (predominantly 2D sheet and flower-like 3D patterns) as revealed by the SEM studies. The co-existence as well as the stability of these nanomorphologies point out towards the intrinsic microheterogeneity prevailing in the IL. Further, the vibrational spectroscopic studies comprising of FT-IR and Raman clearly indicate a sort of accord involving the π-π stacked aromatic geometry and the hydrogen bonding network (between the cation and the anion) of the IL with the CdSe nanoparticles. Therefore, a suitable mechanism has been provided for the resultant anisotropic nanostructures on the basis of the structural and the fluidic aspects of the IL in conjunction with the surface properties of the transient morphologies involved in the process. To further supplement this, control experiments were facilitated by diluting the IL with different amount of water and the morphology of the CdSe nanostructures were examined at respective mole fractions of water as well as at different time intervals.

Keywords: Room temperature ionic liquid, CdSe, Nanoparticle, Microheterogeneity, Anisotropic morphology, Self-assembly.

* Email: asoumya@barc.barc.gov.in, Tel: +91-22-25590301, FAX: +91-22-25505331

Introduction

Room temperature ionic liquids (RTILs) being considered as a potential "green" alternative to traditional organic solvents, have received tremendous attention in various areas of chemistry and industry in recent time. Essentially, RTILs have been widely studied as a reaction media due to their unique physicochemical properties such as high polarity, negligible vapor pressure, high ionic conductivity, and thermal stability.[1-3] Furthermore, alterations in the molecular structure of either the cation or the anion provide a control over the physicochemical properties of the ILs, such as viscosity, solvation, catalytic activity, hydrophobicity and melting points.[4] These features can play a key role in manipulating the application of ILs, which allows these liquids to be designed for specific task. Owing to these properties, RTILs have recently received a great deal of attention as a new media for the synthesis of various nanomaterials and a few reviews regarding the same are available in the literature.[5-7] Various synthetic techniques have been employed for this purpose such as electrodeposition,[8-11] solvothermal,[12-16] sol-gel,[17-19] sonication[20] and radiation induced (e^--beam,[21-23] γ-ray,[24,25] microwave[26-30]) methods. However, reports on IL matrix assisted synthesis of metal chalcogenide nanoparticles that too in *neat* RTILs without the involvement of any stringent experimental conditions are rare.

We wish to report a facile route for the synthesis of CdSe nanoparticles in *neat* RTIL i.e. 1-ethyl-3-methyl imidazolium ethylsulfate ([EMIM][$EtSO_4$]). The molecular structure of the as employed IL has been shown in Fig.1 along with the denotations of various atoms of cation and the anion.

Figure 1

The alkyl sulfate anion based IL (i.e. [EMIM][$EtSO_4$]) was employed as the solvent for synthesis of the nanoparticles. Most commonly used RTILs containing PF_6 and BF_4 anions are vulnerable to hydrolysis in the presence of water and eventually lead to the formation of toxic and corrosive species.[31-33] On the contrary, alkyl sulfate anion based ILs are halogen-free and relatively hydrolysis-stable, providing better alternative for industrial applications.[34] It is to be mentioned here that recently we have reported formation of islands of CdSe nanoparticles within the Se nanofibers, synthesized by electron beam irradiation using the same IL[35] (*neat*) as the solvent. Nanosheets and nanoneedles of CdSe were predominantly formed by using the γ-irradiation method. Undoubtedly, imidazolium based ILs are radiation stable with only a small amount (1mol% or less) of radiolytic degradation.[36] However, in case of imidazolium based FAP (Fluoro alkyl phosphate) ILs,[37] some sort of perturbations in the bonding interactions between the cationic and the anionic moieties were noticed at high radiation doses.[37] Therefore, the other main objective of the present work was to examine the influence of the inherent structure of IL in influencing the morphology of the nanoparticles without perturbing internal structure of the IL by high energy radiation as mentioned. Thus, in the present case synthesis of the nanoparticles was carried out under ambient conditions without using any solvents (for dilution) or stabilizing agent. Of course, control experiments were conducted by diluting the IL with different mole fractions of water and the morphologies obtained were examined. Finally, an attempt has been made to correlate the results with the structural and fluidic aspects of the RTILs.

Experimental

Chemicals

High purity chemicals, cadmium sulfate ($CdSO_4$), Sodium Selenite (Na_2SeO_3), tertiary-butanol were obtained from Sigma-Aldrich and used without further purification. The IL 1-Ethyl-3-

methyl imidazolium ethyl sulfate ([EMIM][$EtSO_4$]) was purchased from Alfa Aesar (UK), with the purity of 99%. The water content in the as employed IL was measured by coulometric Karl-Fischer method using a Metrohm 831 KF Coulometer and was determined to be very less i.e. 20 ppm to cause any considerable changes in the intrinsic structure of the IL. Nanopure water (conductivity, 0.06 μS cm^{-1}) used for washing the precipitates, was obtained from a Millipore water purifying system. Other chemicals such as ethanol used for subsequent cleaning and washing off the organic impurities from the precipitates were obtained from sdfine-chem Ltd. Mumbai, with highest purity.

Instrumentation

The optical absorption spectra were recorded at room temperature using a JASCO V-650 absorption spectrophotometer. Surface and morphological characterization of as obtained nanoparticles were carried out on JEOL JSM-T330 Scanning Electron Microscope (SEM). The transmission electron microscopy (TEM) measurements were acquired on model number FEI, TECNAI-F30. Samples for TEM measurements were prepared by depositing a drop of the nanoparticle solution on thin carbon coated copper grid followed by drying under an IR lamp. X-ray diffraction (XRD) measurements were recorded on a Phillips X-ray diffractometer, model PW 1710 system, using a monochromatic Cu Kα source (λ = 1.54 Å). The instrument was well calibrated using standard samples before any measurements. The FT-IR spectra were recorded using a diamond single reflectance ATR probe in an IR Affinity-1 spectrometer. The compositional analysis of the samples was performed with energy dispersive X-ray spectrometer (EDX), an accessory of SEM (JEOL JSM-T330 SEM). Raman spectral studies were carried out on Seki's STR300 Raman spectrometer using an excitation wavelength of 532 nm from a fibre coupled diode-pumped solid-state laser (DPSS) source. The Raman spectra of the IL and the IL +

CdSe were recorded by putting a drop of the respective sample solutions on a glass slide. The Raman spectra of the precipitates were also recorded (on a Si (Silicon) wafer) to avoid the anticipated interference of the host matrix (i.e. IL) with that of the CdSe.

Synthesis

Briefly, Cadmium sulfate ($CdSO_4$), 0.0156 gm and Sodium selenite (Na_2SeO_3), 0.0129 gm were dissolved in 2.0 ml of IL (1-ethyl-3-methyl imidazolium ethyl sulfate, [EMIM][$EtSO_4$]) by sonication for 30-45 minutes followed by magnetic stirring for nearly 30 minutes. Consecutively, 0.0076 gm of sodium borohydride ($NaBH_4$, SBH) was added to the above solution as a reducing agent, while stirring the same at 1500 rpm (rotations per minute). On mixing, the color of the IL turned to reddish orange within the first 2 minutes of the reaction, and then subsequently changed to yellowish green after 5 minutes, which remained stable for prolonged period of time. The precipitates of the nanoparticles were obtained by centrifugation of the sample at 9000 rpm (rotations per minute) followed by washing the same with ethanol and nanopure water for 3-4 times. The precipitates were utilized for carrying out compositional and morphological characterization studies.

Results and discussion

The UV-Vis absorption spectrum of the yellowish green solution obtained upon mixing of the precursor and $NaBH_4$ provided in Fig.2 clearly shows a shoulder like excitonic peak at ~ 400 nm, while no such spectral feature observed in case of neat IL only.

Figure 2

However, the excitonic peak is quite broad and not very well refined. The large difference between the onset and the shoulder indicates polydispersity in the size or in the shape

distribution of the nanoparticles. Nonetheless, an estimation of the average nanoparticle size of CdSe was calculated using the simplified Brus equation (1).

$$E_g = E_g(0) + \alpha/d^2 \quad (1)$$

Where, α = 3.7 eV nm^2, bulk band gap of CdSe i.e. $E_g(0)$ = 1.75 eV, d = nanoparticle size (nm) and E_g is the band gap value of nanoparticles in eV. The band gap (E_g) value was determined from the Tauc plot of $(\alpha' h\nu)^2$ *vs.* hν, as this is a direct band gap semiconductor (inset of Fig. 2). The symbol 'α'' represents the absorption coefficient multiplied with the concentration of the CdSe nanoparticles, which was obtained from the relation (2.303A/ℓ), where 'A' is the absorbance and 'ℓ' is the optical path length of the cell (10 mm). The term 'hν' represents the photon energy. The estimated average values of the bang gap and the particle size were found to be 2.81 eV and 1.85 nm, respectively, which indicate the strong quantum confinement effect exhibited by the CdSe nanoparticles. The probable reaction of Cd and the Se precursors with the reducing agent ($NaBH_4$) leading to the formation of CdSe nanoparticles can be formulated as follows:

$$4SeO_3^{2-} + 3BH_4^- \rightarrow 4Se^{2-} + 3BO_2^- + 6H_2O \quad (2)$$

$$Se^{2-} + CdSO_4 \rightarrow CdSe\downarrow + SO_4^{2-} \quad (3)$$

The presence of Cd^{2+} ions are expected to be near the anion part ($EtSO_4$) of the IL where as SeO_3^{2-} ions might find its proximity near the EMIM cation (due to the electrostatic forces). Further, the reducing species (BH_4^-) is also expected to be in the close immediacy of the imidazolium cation. Apart from that, the reduction potential of SeO_3^{2-} / Se (E° = -0.37 V *Vs* SHE) is lower than that of Cd^{2+} / Cd (E° = -0.40 V *Vs* SHE). These facts signify the feasibility and the high reactivity of the selenite ions (SeO_3^{2-}) as compare to the cadmium ions (Cd^{2+}), thereby supporting the proposed reactions for the formation of CdSe nanoparticles.

A typical XRD pattern obtained from the as prepared nanoparticles, before and after heating (at 230 °C for 1 hour) has been shown in Fig.3. The unheated one (Fig.3a) shows a broad and noisy spectrum, which makes it difficult to identify the phase of the nanoparticles. However, the heat treatment would have lead to the annihilation of various anticipated organic and inorganic impurities along with the fusion of plausible surface defects present in the form of grain boundaries. This is quite evident from the well-refined diffraction peaks consistent with the wurtzite structure of CdSe (Fig.3b). The lattice constants as determined are: a = 4.284 Å and c = 6.986 Å, which are little lower than the standard value of wurtzite phase of CdSe (a = 4.299 Å and c = 7.010 Å, JCPDS file No. 08-0459). This signifies tensile stress leading to lattice contraction. The peaks marked by the star sign (★) could be probably originated due to presence of residual Se.

Figure 3

The TEM images of the as grown nanoparticles have been shown in Fig.4. The polydispersity in the particle size (2 to 5 nm) could be observed from the HRTEM image shown in Fig.4b. However, average nanoparticle size was found to be ~ 2 nm, which matches well with that estimated from the absorption spectral studies.

Figure 4

More interesting aspect revealed from the TEM studies is the self-assembling of the primary nanoparticles into some sort of superstructures (Fig.4a). Additional TEM images showing similar re-arrangement of the primary nanoparticles have been provided in the supporting information (Fig. S1). Indeed, the self-assembling phenomenon was clearly observed from the TEM images

(Fig. S2 a & b) recorded after 5 hours of the reaction. Consequently, the formation of sheet like superstructures as a result of self-assembling can be realized from the images shown in Fig. S2 c & d. However, the SAED (selected area electron diffraction) pattern (inset of Fig. S2 d) rules out the formation of a single cystalline structures. In fact, the self-assembling behavior of the primary nanoparticles has been demonstrated earlier in RTILs by Zhou *et al*.[19a]

To further probe into the self-assembling of the primary nanoparticles, SEM measurements were recorded at different regions, shown in Fig.5. The composition was analysed by recording the EDX spectrum (inset of Fig.5a), which confirmed the formation of CdSe nanoparticles. The peak showing the presence of Si is originated from Silicon wafer used as a substrate for the sample analysis.

Figure 5

As indicated in Fig.5a, the primary nanoparticles were having nearly globular shape, which grow into nanoflake (NF) like structures and the formation of such features could be clearly seen (depicted by an arrow) in Fig.5b. Subsequently, the NFs self-assemble to form a mixture of nanosheets (2D) and nanoflower (3D) like structures. The formation of both of these anisotropic nanostructures could be clearly noticed in Fig.5c & d as well as after 24 hours of the reaction (Fig.6). It is to be noted that even after 24 hours of the reaction, the morphologies were stable as were found after 5 hours of the reaction. This clearly indicates that IL itself is acting as a good stabilizing agent in maintaining the nanomorphologies unperturbed even after 24 hours of the reaction.

Figure 6

From the SEM images, it can be noticed that the NFs assemble non-homogeneously due to their anticipated high surface area and eventually form the 2D (sheet like) and 3D (flower like) nano or even microarchitectures. The sheets are due to the fusion of NFs at the end, edge and the front facets, thereby resulting into multilayered 2D structures (marked in Fig.5d) with length and width in the range of 10-15 μm and 1-2 μm, respectively. To the best of our knowledge, there has not been any earlier report on the formation and the co-existence of nano/micro-scaled sheets and flowers of CdSe in *neat* ILs. At this stage, it is imperative to recall some of the recent works regarding the synthesis of metal chalcogenide nanoparticles assisted by ILs. For instance, the preparation of ZnS nanoparticles,[38a] flower like MoS_2,[38b] PbS nanocubes,[38c] ZnSe hollow microspheres [38d] and CdSe hierarchical dendrites [38e] have been reported with the *aid* of ILs. As could be noticed that predominantly single morphologies have been mentioned in these reports and none of these accounts for the simultaneous co-existence of different nanomorphologies as observed in the present case. Moreover, the synthetic protocols of these nano/microstructures involved conventional solvents for dilution purpose in conjugation with the employment of high temperature/pressure techniques (i.e. autoclaving). Presumably, the intrinsic networking structure of the IL would have perturbed in such conditions. Still, some of the nanostructures were found to be hierarchical (self-assembly of primary units) in nature, which have been explained rendering the influence/presence of the ILs employed therein. To provide a precise mechanism for the formation of anisotropic nanostructures as obtained in the present case may not be easy. However, a possible explanation might be given on the basis of the inherent structural and fluidic aspects of the IL (compared to the conventional solvents) in the initial phase of the reaction i.e. up to the formation of nanoflakes. These nanoflakes with high energy surfaces are combined together to form nano/micro sheets and flower like structures, which are found to co-exist and

stabilized by the rigid structure of IL. The viscosity of the IL, [EMIM][$EtSO_4$] is ~ 100.4 cP at 298.15 K,[39] which is at least 10 times higher as compared to usually employed conventional solvents (aqueous and organic) for the synthesis of nanoparticles. Such high viscosity would significantly slow down the diffusion of the reactant ions as well as the primary nanospecies. In other words, compared to the fast nucleation and aggregation in the conventional solvents, the primary CdSe nanospecies would be kinetically slower, thereby allowing them to have enough time to grow into hierarchical morphologies directed by the networking structure of the IL. Moreover, RTILs display a high degree of self-organization and microheterogeneity in the liquid state.[40] It has been shown, both by theoretical and experimental studies that a three-dimensional ionic network dominated by the electrostatic interactions co-exists with non-polar domains in these media.[41-44] Besides, ILs comprises of extended hydrogen bonding systems[45] and are therefore, highly structured.[46, 47] This can be envisaged from the fact that imidazolium based ILs comprises of non-covalent bonding interactions such as π-π stacked aromatic geometry among the cationic moieties.[48] Consequently, this feature along with the extended hydrogen bonding network (*hydrogen bond-co-π-π stacking mechanism*) has been regarded as the shape directing mechanism for obtaining various anisotropic structures (tubes, wires, rods, sheets) of nanomaterials synthesized in imidazolium based ILs, by different techniques.[48c, 49]Apparently, the relative diffusion flux (in various domains of ILs; structural heterogeneity) complemented by the diffusion limited aggregation (fluidic aspect of the ILs) of the nanospecies formed at the initial stages could be regarded as the possible factors for their self-organization process. However, as the inherent heterogeneity of the IL is in nanoscale, it cannot be responsible for microstructures as obtained in the present case. It is well known fact that the thermodynamic processes often result in uniform growth of all crystal facets and subsequent formation of

spherical or near spherical structures.[50b] Whereas, preferential and directional growth occurs in case of kinetically controlled process resulting into the formation of various anisotropic nanostructures. In other words, if the enthalpy gain from such oriented attachment dominates the entropy loss, the self assembled 2D or the 3D nanostructures could become thermodynamically favorable.[51] The driving force for such process is the elimination of the high energy surfaces, ultimately leading to a substantial reduction in the surface free energy. Thus, in the present case, the nanoflakes self-assemble in different ways to generate the anisotropic structures.

In the conventional organic and aqueous solvents some ligands/external templates/ matrix has to be incorporated into the reaction system to stabilize the nanomaterials or direct their shape. Further, the synthesis of nanomaterials in conventional solvents is generally carried out at high temperatures, pressures or inert atmospheres. The property of the nanomaterials also strongly depends on the synthetic conditions, ligands and templates used in the reaction mixture. Therefore, it would be very difficult to compare the structures and properties of nanomaterials prepared in the RTIL with those prepared in conventional solvents. Nevertheless, some control experiments were carried out by diluting the IL with water, keeping other experimental parameters unchanged. In such two cases, mole fraction of water in the reaction mixtures were 0.35 and 0.91, and the respective morphologies of the CdSe nanoparticles were examined. It is clearly evident from Fig.7 that at 0.35 mole fractions of water, the nanostructure as well as their distribution is significantly different from the former case (*neat* IL). Interestingly, the 3D flower like morphology was formed predominantly due to the self-assembly of NFs (see Fig.7c & d).

Figure 7

Furthermore, the large sheet like morphologies formed through the fusion of NFs (as in case of *neat* ILs) were not observed in this case. Instead, the small sheet-like units (NFs) having the length primarily in the range of 2-5 μm were found to be fused by their tails, while the other side remained free. This orientation gives the impression of the flower like morphology with petals comprising a bunch of well aligned NFs. On the contrary, the NFs (primary units) forming the flower like nano/microstructures in case of *neat* IL were found to orient randomly.

After 24 hours of the reaction, the morphology of the CdSe nanostructures was re-examined and the SEM images are shown in Fig.8.

Figure 8

Mainly nanoneedles accompanied by nanorods and nanosheets are visible, while no flower like architectures were noticed in this case. Indeed, this transformation of 3D nanomorphology into a mixture of 1D and 2D nanostructures was surprising. However, the plausible reason behind this transition could be the combined effect of structural defects present in the initial morphology as well as the decline in the stabilizing tendency of the host matrix i.e. IL with the presence of water. Images shown in Fig.7 indicates that the petals (NFs) are well aligned leading to the formation of a flower like geometry but some defects due to the minor distortion in their arrangements at some places could be noticed very clearly. Such defects may induce the instability in the structure and thus encourage its transformation to other morphologies.[50a] It is to be mentioned here that the presence of such structural defects cannot be denied in case of nanoflowers formed in *neat* IL. But, no such structural transition was observed in that case which could be due to the inherent rigidity present in the host matrix of IL.

Similar structural transformation with different nanomorphologies was observed on further dilution of the IL (mole fraction of water = 0.91). The nanoparticles formed in this case underwent coagulation followed by precipitation within few minutes of the reaction. Nonetheless, flower like morphologies were observed in various regions of the sample, as could be seen from the SEM images recorded after 5 hours of the reaction (Fig.9 and Fig.S3).

Figure 9

It can be noticed that the irregular alignment and random fusion of NFs, needles and some fiber like nanoscale units actually gave the distorted flower like structures (Fig.S3.c & d). These flower like morphologies were not predominant after 24 hours, rather the nanoscale units i.e. NFs, rods and needles were present in a non-uniform and random manner (Fig.10). Furthermore, these anisotropic nanoscale units were not found to fuse into each other and primarily joined at their heads and tails. But, in case of *neat* IL, the NFs were fused into each other to form sheets of microscale dimensions, as already discussed.

Figure 10

It is essential and worthwhile to mention here that the dimension of the anisotropic (1D or 2D) nano/microarchitectures decreases with the increase in the volume fraction of water. Unambiguously, the IL still influences the morphology of the CdSe nanoparticles, but its shape directing and stabilizing tendencies appeared to be considerably declined. The plausible reason for this is ascribed due to the perturbation of the internal structural organization of the IL, which causes a decrease in the extended ordering of nanoscale structures. In other words, the self-assembling tendency of the primary units weakened with the dilution of the IL. Although, self-

assembled 3D nano/microstructures were observed (Fig.7) at 0.35 mole fraction of water, but these were transient stages which eventually transformed into predominantly well separated 1D anisotropic structure (Fig.8). A probable scheme depicting the formation of these anisotropic nanomorphologies of CdSe along with the different intermediate stages has been shown in Fig.11. The proposed scheme, based on results obtained and available literature appears to be reasonable at this point of time however, provides scope for refinement by future research.

Figure 11

Further characterization of the as grown CdSe nanoparticles was carried out by recording the Raman spectrum of the precipitates extracted from the IL. Fig.12 shows the Raman spectrum of the precipitates with multi-Lorentzian fitting. As could be seen, the spectrum comprises of fundamental longitudinal optical (LO) phonon peak along with its overtone (2LO) peak at ~ 205 cm^{-1} and ~ 408 cm^{-1}, respectively. A shoulder near 170 cm^{-1} can be noticed, which is attributed to the transverse optical (TO) phonon mode of CdSe nanoparticles.[52] A small and broad peak at about 264 cm^{-1} is also apparent in the spectrum.

Figure 12

Essentially, appearance of surface optic (SO) modes has been reported earlier [53] in case of small sized quantum dots (CdSe) accompanied by a peak near 250 cm^{-1}. And these SO modes originates due to the presence of more number of atoms on the surface as compare to the bulk in very small sized nanoclusters, behaving like molecules.[53] Similar band was observed by Epifani *et al.*[52] in case of CdSe nanoparticles at around 270 cm^{-1} and was assigned to the SO modes. Furthermore, the presence of amorphous-Se has also been reported to exhibit a Raman peak at

around 264 cm^{-1}.[54] The data obtained from the EDX analysis seems to corroborate well with the possibility of the existence of more number of Se atoms on the surface of the nanoparticles. Thus, the peak obtained at about 264 cm^{-1} in the Raman spectrum of as grown CdSe nanoparticles has been attributed to the SO modes. This is further substantiated by the signatures of the Se-O bond formation (discussed later) in the Raman spectral analysis of IL containing CdSe. The peak at around 346 cm^{-1} could be ascribed to the 2TO phonon mode of the CdSe similar to that assigned by Venugopal *et al.*[55] for the 2TO phonon modes (at ~ 356.8 cm^{-1}) of CdSe nanobelts. Besides, a red shift (down shift) of LO peak from its position for bulk CdSe (of 210 - 213 cm^{-1}) [56] was also observed. The reduction in size of various materials is mainly dominated by quantum confinement effects, but it is often accompanied by the dimensional effects such as surface reconstruction and lattice contraction. These dimensional effects arise due to the variation in surface energy which is a function of particle size. As a result of reduced dimensions, a competition between strain and confinement effects exists. Therefore, when a crystal with reduced dimensions experiences phonon confinement or tensile stress (strain effect), optical phonon modes undergo red shift with respect to their bulk values.[56a] Considering this, the red shift observed in our case has been attributed due to the phonon confinement effect as the size of the primary nanoparticles were between 2 to 5 nm (from HRTEM), which is less than the bulk Bohr exciton radius of CdSe (5.6 nm).[57] Therefore, the down shift in the LO peak relative to the bulk value appears to be the combined effect of the phonon confinement and the strain leading to the tensile stress, as observed in XRD also.

FT-IR spectral studies were carried out to probe the perturbations in the bonding interactions of the cationic and the anionic moieties of the IL pertaining to the formation of CdSe

nanoparticles. The IR spectra of the neat as well as the IL containing CdSe have been shown in Fig.13.

Figure 13

It is to be mentioned here that detail vibrational studies (involving IR and Raman) of [EMIM][$EtSO_4$] have been reported earlier by Kiefer *et al.*[58a] and other researchers.[58b] The theoretical as well as experimentally determined vibrational frequencies of various bonds of the IL have been reported therein. In the present work, the IR spectra of IL and IL + CdSe (Fig.13a & b) do not exhibit any significant difference, especially in the region of 4000-700 cm^{-1}. However, in the range of 700-500 cm^{-1} (inset of Fig.13) considerable changes in the vibrational frequencies of the IL containing CdSe with respect to the relative intensities as well as in the peak positions were observed. The intensities of the peaks with wave numbers 648 cm^{-1} and 617 cm^{-1} representing the ring out-of-plane asymmetric bending vibrations[58a] decrease in case of IL + CdSe as compared to the neat IL. Dhumal *et al.*[58b] have assigned the peak at 648 cm^{-1} to the CN bond oscillation. Similar bending vibrations at ~ 600 cm^{-1} were diminished considerably in case of IL + CdSe as compared to the *neat* one. Further, the peak position of the vibrational frequency at ~ 565 cm^{-1} (due to the ring in-plane symmetric bending[58a] for *neat* IL) was red shifted (change of ~ 2cm^{-1}) in the presence of CdSe (i.e. IL + CdSe). All these signify the interaction prevailing between the imidazolium cation and the CdSe nanoparticles. In addition, the peak at ~ 517 cm^{-1} (for *neat* IL) representing the bending vibrational mode of bond $O_{[3]}$-$S_{[1]}$-$O_{[5]}$ [58b] decreases significantly in case of IL + CdSe. These observations clearly indicate that both the imidazolium cation and the ethylsulfate anion are involved in the interaction with the CdSe nanoparticles. Some earlier studies related to the synthesis of various nanomaterials in ILs satisfactorily

corroborate our findings. For instance, Dupont *et al.*[16b] demonstrated that the interaction between the metal surface and the IL is through oxygen in case of triflate, CF_3SO_3 or through F (in case of anions i.e. BF_4 / PF_6) as anion. Zhou *et al.* [48c] reported the synthesis of monolithic mesoporous silica with wormhole framework and attributed its formation mechanism to both the hydrogen bonds formed between the anionic moiety of the IL and the silano group of silica gel and the π–π stacking interactions between the neighboring imidazolium rings. These interactions were confirmed by employing the FT-IR spectroscopy.

Raman spectroscopy being a complementary technique to the IR spectroscopy was employed to examine the alterations in the vibrational frequencies of the IL in the presence of CdSe. Raman spectra of the *neat* IL and the IL + CdSe have been shown in Fig.14.

Figure 14

The spectrum of the *neat* IL matches well with the earlier reports.[58] The Raman spectra of the *neat* IL resembles closely with that of IL + CdSe with the appearance of some new peaks in the later case. No significant vibrations in the region of 1600-2600 cm^{-1} could be observed in case of neat IL as well as in the presence of CdSe. While, some peaks were observed (as per the earlier reports[58]) in the region of 2900-3200 cm^{-1}, no major change could be noticed in both the cases (shown in Fig.S4). The peak at ~ 205 cm^{-1} (peak [1], IL + CdSe) (Fig.14b) have been assigned to the fundamental LO phonon mode of the CdSe. Additional peak at 854 cm^{-1} (shown as peak [4]) could be observed only in case of IL + CdSe and has been ascribed to the formation of a Se–O bond.[59] The peaks present in the region 710-770 cm^{-1} represents the C-C stretching and the ring HCCH symmetric bending modes of the *neat* IL, [58a] which are altered and broadened in case of IL + CdSe (marked as [3]). Further, the peak appearing at ~ 250 cm^{-1} in case of *neat* IL (ascribed

to the out-of-plane bending mode of the CH_3-(N) methyl group in the imidazolium cation[60]) is perturbed in case of IL + CdSe and seems to be embedded due to the appearance of a hump extending from 250-270cm^{-1} (marked as [2]). The presence of amorphous-Se might have contributed to the broadening in the aforesaid region as has been observed (Fig.12) in case of CdSe nanoparticles extracted from the IL. It is reasonable to confer that these variations in the intensities and the positions of the vibrational peak frequencies clearly indicate the involvement of π-π stacked aromatic geometry (among the cationic moieties) and the hydrogen bonding network (between the cation and the anion) is responsible for the as obtained nanomorphologies.

Figure 15

A pictorial representation of the interactions among the cationic and the anionic moieties of the IL with CdSe on the basis of the vibrational studies are shown in Fig.15.

Conclusions

In the present work, we demonstrated the influence of the inherent structure of the RTIL on the morphology of CdSe nanoparticles synthesized at purely ambient conditions. It was observed that IL played multiple roles i.e. a solvent, stabilizing agent and a shape directing template. The fluidic aspects of the IL in conjunction with its *hydrogen bond-co-π-π stacking* mechanism enabled it to perform a function of a diffusion controller and an anisotropic growth director, respectively. Moreover, the vibrational spectroscopic studies involving FT-IR and Raman clearly indicated a sort of accord involving the π-π stacked aromatic geometry (among the cationic moieties) and the hydrogen bonding network (between the cation and the anion) with the CdSe nanoparticles. Presumably, the co-existence of the as obtained anisotropic 2D and 3D nano/microstructures has been accredited to the interplay of both unique structural and the fluidic

aspects of the as employed RTIL in combination with the surface related energetics of the transient morphologies involved in the process. Furthermore, the current study on one hand categorically demonstrates and emphasizes the fundamental role of water in creating the perturbations/distortions in the networking structure of the IL but also reflect the potential to maneuver the morphologies of the nanomaterials by precisely controlling the presence of water in the host matrix of IL. However, further investigations are essential for the better understanding of the role of intrinsic microheterogeneity prevailing in the RTILs so that these media could be used as templates in fine tuning the morphology of the nanoparticles which in turn is associated to their properties and applications.

Acknowledgement

The authors acknowledge Mr. Jitendra Nuwad and Dr. S. N. Achary of Chemistry Division for the SEM and XRD measurements, respectively. The authors would like to thank Mr. R. S. Gholap, National Chemical Laboratory, Pune for his help in TEM measurements. The FTIR measurements carried out by Mr. K. K. Singh is thankfully acknowledged. The SEM facility provided by G&ACD is gratefully acknowledged. We thank Dr. D. K. Palit, Head, RPCD and Dr. B. N. Jagatap, Director, Chemistry group of Bhabha Atomic Research Centre of Mumbai for their encouragement and support.

References

1. T. Welton, *Chem. Rev.*, 1999, **99**, 2071–2083.
2. V. I. Pârvulescu and C. Hardacre, *Chem. Rev.*, 2007, **107**, 2615–2665.
3. J. P. Hallett and T. Welton, *Chem. Rev.*, 2011, **111**, 3508–3576.
4. (a) J. D. Holbrey and K. R. Seddon, *Clean Technol. Environ. Policy*, 1999, **1**, 223–236; (b) L. C. Branco, J. N. Rosa, J. J. Moura Ramos, and C. A. M. Afonso, *Chem. Eur. J.*, 2002, **8**, 3671–3677; (c) J. H. Werner, S. N. Baker, and G. A. Baker, *Analyst*, 2003, **128**, 786–789; (d) S. N. Baker, G. A. Baker, and F. V. Bright, *Green Chem.*, 2002, **4**, 165–169; (e) A. E. Bradley, C. Hardacre, J. D. Holbrey, S. Johnston, S. E. J. McMath, and M. Nieuwenhuyzen, *Chem. Mater.*, 2002, **14**, 629–635; (f) S. V Dzyuba and R. A. Bartsch, *Chemphyschem*, 2002, **3**, 161–166; (g) J. L. Anthony, E. J. Maginn, and J. F. Brennecke, *J. Phys. Chem. B*, 2001, **105**, 10942–10949; (h) H. L. Ngo, K. LeCompte, L. Hargens, and A. B. McEwen, *Thermochim. Acta*, 2000, **357-358**, 97–102.
5. Z. Li, Z. Jia, Y. Luan, and T. Mu, *Curr. Opin. Solid State Mater. Sci.*, 2008, **12**, 1–8.
6. M. Antonietti, D. Kuang, B. Smarsly, and Y. Zhou, *Angew. Chem. Int. Ed. Engl.*, 2004, **43**, 4988–92.
7. Z. Ma, J. Yu, and S. Dai, *Adv. Mater.*, 2010, **22**, 261–85.
8. F. Endres, M. Bukowski, R. Hempelmann, and H. Natter, *Angew. Chem. Int. Ed. Engl.*, 2003, **42**, 3428–30.
9. S. Zein El Abedin, N. Borissenko, and F. Endres, *Electrochem. commun.*, 2004, 6, 510–514.
10. J.-F. Huang and I.-W. Sun, *Adv. Funct. Mater.*, 2005, **15**, 989–994.
11. J.-F. Huang and Sun I-Wen, *Chem. Mater.*, 2004, **16**, 1829–1831.

12. H. G. Zhu, J. F. Huang, Z. W. Pan, and S. Dai, *Chem. Mater.*, 2006, **18**, 4473–4477.

13. Y. Wang and H. Yang, *J. Am. Chem. Soc.*, 2005, **127**, 5316–5317.

14. Y. Wang and H. Yang, *Chem. Commun.*, 2006, 2545–2547.

15. X. Zhou, Z.-X. Xie, Z.-Y. Jiang, Q. Kuang, S.-H. Zhang, T. Xu, R.-B. Huang, and L.-S. Zheng, *Chem. Commun.*, 2005, 5572–5574.

16. (a) J. Jiang, S. Yu, W. Yao, H. Ge, and G. Zhang, *Chem. Mater.*, 2005, **17**, 6094–6100; (b) G. S. Fonseca, G. Machado, S. R. Teixeira, G. H. Fecher, J. Morais, M. C. M. Alves, and J. Dupont, *J. Colloid Interface Sci.*, 2006, **301**, 193–204.

17. S. Dai, Y. H. Ju, H. J. Gao, J. S. Lin, S. J. Pennycook, and C. E. Barnes, *Chem. Commun.*, 2000, 243–244.

18. T. Nakashima and N. Kimizuka, *J. Am. Chem. Soc.*, 2003, **125**, 6386–6387.

19. (a) Y. Zhou and M. Antonietti, *J. Am. Chem. Soc.*, 2003, **125**, 14960–14961; (b) T. Wagner, S. Haffer, C. Weinberger, D. Klaus, and M. Tiemann, *Chem. Soc. Rev.*, 2013, **42**, 4036–4053; (c) K. Ariga, V. Ajayan, Y. Yamauch, Q. Ji, and P. H. Jonathan, *Bull. Chem. Soc. Jpn.*, 2012, **85**, 1–32.

20. E. K. Goharshadi, Y. Ding, M. N. Jorabchi, and P. Nancarrow, *Ultrason. Sonochem.*, 2009, **16**, 120–123.

21. T. Tsuda, T. Sakamoto, Y. Nishimura, S. Seino, A. Imanishi, and S. Kuwabata, *Chem. Commun.*, 2012, **48**, 1925.

22. T. Tsuda, T. Sakamoto, Y. Nishimura, S. Seino, A. Imanishi, K. Matsumoto, R. Hagiwara, T. Uematsu, and S. Kuwabata, *RSC Adv.*, 2012, **2**, 11801–11807.

23. A. Imanishi, T. Masaaki, and S. Kuwabata, *ChemComm*, 2009, 1775–1777.

24. S. Chen, Y. Liu, and G. Wu, *Nanotechnology*, 2005, **16**, 2360–2364.

25. M.-E. Meyre, M. Tréguer-Delapierre, and C. Faure, *Langmuir*, 2008, **24**, 4421–5.

26. Z. Li, Z. Liu, J. Zhang, B. Han, J. Du, Y. Gao, and T. Jiang, *J. Phys. Chem. B*, 2005, **109**, 14445–8.

27. Y. Jiang, Y.-J. Zhu, and G.-F. Cheng, *Cryst. Growth Des.*, 2006, **6**, 2174–2176.

28. Y. Jiang and Y.-J. Zhu, *J. Phys. Chem. B*, 2005, **109**, 4361–4.

29. L.-X. Yang, Y.-J. Zhu, W.-W. Wang, H. Tong, and M.-L. Ruan, *J. Phys. Chem. B*, 2006, **110**, 6609–6614.

30. Z. Liu, Z. Sun, B. Han, J. Zhang, J. Huang, J. Du, and S. Miao, *J. Nanosci. Nanotechnol.*, 2006, **6**, 175–179.

31. F. Endres and S. Zein El Abedin, *Phys. Chem. Chem. Phys.*, 2006, **8**, 2101–16.

32. J. H. Porada, M. Mansueto, S. Laschat, and C. Stubenrauch, *Soft Matter*, 2011, **7**, 6805–6810.

33. S. Keskin, D. Kayrak-Talay, U. Akman, and Ö. Hortaçsu, *J. Supercrit. Fluids*, 2007, **43**, 150–180.

34. P. Wasserscheid, R. Van Hal, and A. Bösmann, *Green Chem.*, 2002, **4**, 400–404.

35. A. Guleria, A. K. Singh, M. C. Rath, S. Adhikari, and S. K. Sarkar, *Dalton Trans.*, 2013, **42**, 15159–68.

36. (a) D. Allen, G. Baston, A. E. Bradley, T. Gorman, A. Haile, I. Hamblett, J. E. Hatter, M. J. F. Healey, B. Hodgson, R. Lewin, K. V. Lovell, B. Newton, W. R. Pitner, D. W. Rooney, D. Sanders, K. R. Seddon, H. E. Sims, and R. C. Thied, *Green Chem.*, 2002, **4**, 152–158; (b) L. Berthon, S. I. Nikitenko, I. Bisel, C. Berthon, M. Faucon, B. Saucerotte, N. Zorz, and P. Moisy, *Dalton Trans.*, 2006, 2526–34; (c) M. Qi, G. Wu, S. Chen, and Y. Liu, *Radiat. Res.*, 2007, **167**, 508–14; (d) M. Qi, G. Wu, Q. Li, and Y. Luo, *Radiat. Phys.*

Chem., 2008, **77**, 877–883; (e) L. Yuan, J. Peng, M. Zhai, J. Li, and G. Wei, *Radiat. Phys. Chem.*, 2009, **78**, 737–739; (f) G. Le Rouzo, C. Lamouroux, V. Dauvois, A. Dannoux, S. Legand, D. Durand, P. Moisy, and G. Moutiers, *Dalt. Trans.*, 2009, 6175–84; (g) L. Yuan, J. Peng, L. Xu, M. Zhai, J. Li, and G. Wei, *Radiat. Phys. Chem.*, 2009, **78**, 1133–1136; (h) C. Jagadeeswara Rao, K. a. Venkatesan, B. V. R. Tata, K. Nagarajan, T. G. Srinivasan, and P. R. Vasudeva Rao, *Radiat. Phys. Chem.*, 2011, **80**, 643–649.

37. A. Guleria, A. K. Singh, S. Adhikari, and S. K. Sarkar, *Dalton Trans.*, 2014, **43**, 609–25.

38. (a) Y. Wu, X. Hao, J. Yang, F. Tian, and M. Jiang, *Mater. Lett.*, 2006, 60, 2764–2766; (b) H. Li, W. Li, L. Ma, W. Chen, and J. Wang, *J. Alloys Compd.*, 2009, **471**, 442–447; (c) X.-L. Zhao, C.-X. Wang, X.-P. Hao, J.-X. Yang, Y.-Z. Wu, Y.-P. Tian, X.-T. Tao, and M.-H. Jiang, *Mater. Lett.*, 2007, **61**, 4791–4793; (d) X. Liu, J. Ma, P. Peng, and W. Zheng, *Mater. Sci. Eng. B*, 2008, **150**, 89–94; (e) X. Liu, R. Liu, S. Chen, and B. Liang, *Mater. Lett.*, 2012, **66**, 264–266

39. G. Yu, X. Li, X. Liu, C. Asumana, and X. Chen, *Ind. Eng. Chem. Res.*, 2011, **50**, 2236–2244.

40. (a) T. Ichikawa, M. Yoshio, A. Hamasaki, T. Mukai, H. Ohno, and T. Kato, *J. Am. Chem. Soc.*, 2007, **129**, 10662–10663; (b) T. Gutel, J. Garcia-Antõn, K. Pelzer, K. Philippot, C. C. Santini, Y. Chauvin, B. Chaudret, and J.-M. Basset, *J. Mater. Chem.*, 2007, 17, 3290; (c) L. V. Zherenkova and P. G. Khalatur, *Russ. J. Phys. Chem. A*, 2010, **84**, 1097–1103; (d) Y. Wang and G. A. Voth, *J. Am. Chem. Soc.*, 2005, **127**, 12192–3; (e) Z. Hu and C. J. Margulis, *Proc. Natl. Acad. Sci. U. S. A.*, 2006, **103**, 831–6; (f) A. Samanta, *J. Phys. Chem. B*, 2006, **110**, 13704–13716; (g) H. Jin, X. Li, and M. Maroncelli, *J. Phys. Chem. B*, 2007, **111**, 13473–8; (h) J. Habasaki and K. L. Ngai, *J. Chem. Phys.*, 2008, **129**,

194501–194515; (i) S. G. Raju and S. Balasubramanian, *Indian J. Chem.*, 2010, **49A**, 721–726; (j) S. S. Sarangi, W. Zhao, F. Müller-Plathe, and S. Balasubramanian, *Chemphyschem*, 2010, **11**, 2001–10; (k) S. Patra and A. Samanta, *J. Phys. Chem. B*, 2012, **116**, 12275–83.

41. J. N. A. Canongia Lopes and A. A. H. Pádua, *J. Phys. Chem. B*, 2006, **110**, 3330–5.

42. A. Triolo, O. Russina, H.-J. Bleif, and E. Di Cola, *J. Phys. Chem. B*, 2007, **111**, 4641–4644.

43. A. A. H. Pádua, M. F. Costa Gomes, and J. N. A. Canongia Lopes, *Acc. Chem. Res.*, 2007, **40**, 1087–1096.

44. M. G. Del Pópolo, C. L. Mullan, J. D. Holbrey, C. Hardacre, and P. Ballone, *J. Am. Chem. Soc.*, 2008, **130**, 7032–41.

45. A. Elaiwi, P. B. Hitchcock, K. R. Seddon, N. Srinivasan, Y.-M. Tan, T. Welton, and J. A. Zora, *J. Chem. Soc. Dalt. Trans.*, 1995, **21**, 3467.

46. A. Mele, C. D. Tran, and S. H. D. P. Lacerda, *Angew. Chem. Int. Ed.*, 2003, **42**, 4364–4366.

47. S. Saha, S. Hayashi, A. Kobayashi, and H. Hamaguchi, *Chem. Lett.*, 2003, **32**, 740–741.

48. (a) L. Wu, J. Lian, G. Sun, X. Kong, and W. Zheng, *Eur. J. Inorg. Chem.*, 2009, **2009**, 2897–2900; (b) Z. Li, Z. Jia, Y. Luan, and T. Mu, *Curr. Opin. Solid State Mater. Sci.*, 2008, **12**, 1–8; (c) Y. Zhou, J. H. Schattka, and M. Antonietti, *Nano Lett.*, 2004, **4**, 477–481.

49. (a) Y.-J. Zhu, W.-W. Wang, R.-J. Qi, and X.-L. Hu, *Angew. Chem. Int. Ed.*, 2004, **43**, 1410–4; (b) K. Biswas and C. N. R. Rao, *Chem. Eur. J.*, 2007, **13**, 6123–9; (c) Y. Sun and

W. Zheng, *Dalton Trans.*, 2010, **39**, 7098–103; (d) L. Wang, L. Chang, B. Zhao, Z. Yuan, G. Shao, and W. Zheng, *Inorg. Chem.*, 2008, **47**, 1443–52.

50. (a) J. Ning, K. Men, G. Xiao, L. Wang, Q. Dai, B. Zou, B. Liu, and G. Zou, *Nanoscale*, 2010, **2**, 1699–1703; (b) P. R. Sajanlal, T. S. Sreeprasad, A. K. Samal, and T. Pradeep, *Nano Rev.*, 2011, **2**, 1–62.

51. R. Thiruvengadathan, V. Korampally, A. Ghosh, N. Chanda, K. Gangopadhyay, and S. Gangopadhyay, *Rep. Prog. Phys.*, 2013, **76**, 066501.

52. M. Epifani, E. Pellicer, J. Arbiol, N. Sergent, T. Pagnier, and J. R. Morante, *Langmuir*, 2008, **24**, 11182–8.

53. B. K. Rai, H. D. Bist, R. S. Katiyar, M. T. S. Nair, P. K. Nair, and A. Mannivannan, *J. Appl. Phys.*, 1997, **82**, 1310–1319.

54. (a) B. Gates, B. Mayers, B. Cattle, and Y. Xia, *Adv. Funct. Mater.*, 2002, **12**, 219–227; (b) L. Liu, Q. Peng, and Y. Li, *Nano Res.*, 2008, **1**, 403–411.

55. R. Venugopal, P.-I. Lin, C.-C. Liu, and Y.-T. Chen, *J. Am. Chem. Soc.*, 2005, **127**, 11262–8.

56. (a) R. Meulenberg, T. Jennings, and G. Strouse, *Phys. Rev. B*, 2004, **70**, 235311; (b) A. Tanaka, S. Onari, and T. Arai, *Phys. Rev. B*, 1992, **45**, 6587–6592.

57. R. W. Meulenberg, J. R. I. Lee, A. Wolcott, J. Z. Zhang, L. J. Terminello, and T. van Buuren, *ACS Nano*, 2009, **3**, 325–30.

58. (a) J. Kiefer, J. Fries, and A. Leipertz, *Appl. Spectrosc.*, 2007, **61**, 1306–1311; (b) N. R. Dhumal, H. J. Kim, and J. Kiefer, *J. Phys. Chem. A*, 2011, **115**, 3551–3558.

59. G. Lefèvre, *Adv. Colloid Interface Sci.*, 2004, **107**, 109–123.

60. A. Wulf, K. Fumino, R. Ludwig, and P. F. Taday, *ChemPhysChem*, 2010, **11**, 349–53.

Caption for Figures

Fig.1. Structure of IL, 1-ethyl-3-methyl imidazolium ethylsulfate ([EMIM][$EtSO_4$]).

Fig.2. UV-Vis absorption spectra of *neat* IL (a) and CdSe nanoparticles synthesized in IL ([EMIM][$EtSO_4$]) (b). Inset: Tauc plot of $(\alpha' h\nu)^2$ vs. $h\nu$ for the determination of band gap values (E_g).

Fig.3. XRD spectrum of as grown nanoparticles synthesized in IL ([EMIM][$EtSO_4$]) before (a) and after heating the sample at 230 $^{\circ}$C for 1 hour (b). The peaks marked by the star sign (★**)** has been identified as originated due to presence of residual Se.

Fig.4. TEM **(a)** (*Scale bar dimensions = 50 nm*) and the HRTEM **(b)** image (*Scale bar dimensions = 2 nm*) of the CdSe nanoparticles synthesized in *neat* IL ([EMIM][$EtSO_4$]). Inset in the image (b) shows the lattice fringe pattern with the interplanar distance of 0.18 nm, which correspond to the (201) plane (standard value of the interplanar distance = 0.179 nm) of the hexagonal phase of CdSe.

Fig.5. SEM images of as grown CdSe nanostructures after 5 hours of the reaction at different regions of the sample depicting the various transient stages as: globular like shape (a), nanoflake (NF) like structure (b), flower-like 3D pattern (c) and nanosheet like 2D structures (d). (*Scale bar dimensions in all the images is 3μm*). Inset of image 5a shows the EDX spectrum confirming the formation of CdSe nanoparticles.

Fig.6. SEM images of as grown CdSe nanostructures after 24 hours, showing the dual co-existence of nanosheets and nanoflowers. (*Scale bar dimensions in image (a) is 10 μm and in image (b) is 3μm*).

Fig.7. SEM images (at different regions with various nanoscale dimensions) of as grown CdSe nanostructures synthesized in IL ([EMIM][$EtSO_4$]) having 0.35 mole fraction of water. The

images were taken after 5 hours of the reaction. (*Scale bar dimensions in image (a) = 100 μm, image (b) = 50μm, image (c) & (d) = 10μm*)

Fig.8. SEM images (at different regions with various nanoscale dimensions) of as grown CdSe nanostructures synthesized in IL ([EMIM][$EtSO_4$]) having 0.35 mole fraction of water. The images were taken after 24 hours of the reaction. (*Scale bar dimensions in image (a) & (b) is 10 μm*)

Fig.9. SEM image of as grown CdSe nanostructures synthesized in IL ([EMIM][$EtSO_4$]) having 0.91 mole fraction of water. The image were taken after 5 hours of the reaction. Scale bar dimensions = 5 μm.

Fig.10. SEM images at different nanoscale dimensions of as grown CdSe nanostructures synthesized in IL ([EMIM][$EtSO_4$]) having 0.91 mole fraction of water.

Fig.11. Schematic representation showing the probable intermediate stages with different nano/micromorphologies of CdSe synthesized in IL ([EMIM][$EtSO_4$]), at various time intervals and mole fractions of water.

Fig.12. Multi-Lorentzian fitting Raman spectrum of CdSe nanoparticles synthesized in *neat* IL ([EMIM][$EtSO_4$]).

Fig.13. FT-IR spectra of *neat* IL (a) and IL + CdSe (b). Inset shows the IR spectra of the same in the region of 700-500 cm^{-1}.

Fig.14. Raman spectra of neat IL (a) and IL + CdSe (b). The peaks marked have been described in the text.

Fig.15. The pictorial representation of the possible interactions among the cationic and the anionic moieties of the IL with CdSe nanoparticles.

Figures

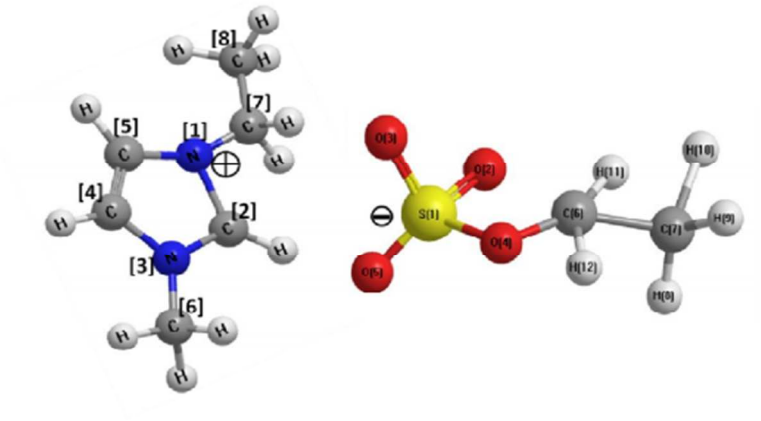

Fig.1

Apurav *et al.*

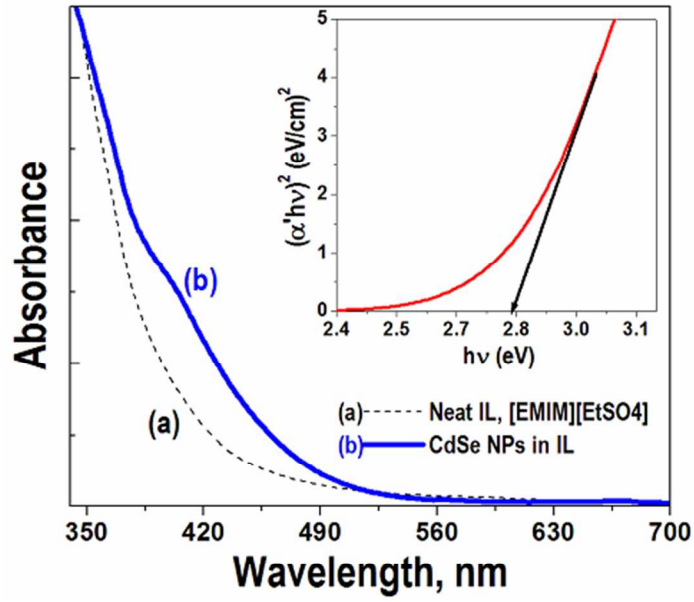

Fig.2

Apurav *et al.*

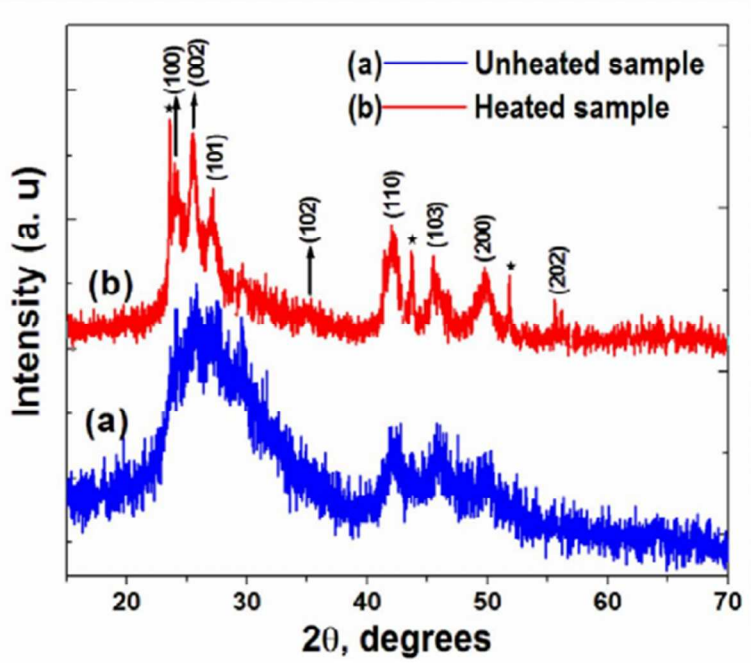

Fig.3

Apurav *et al.*

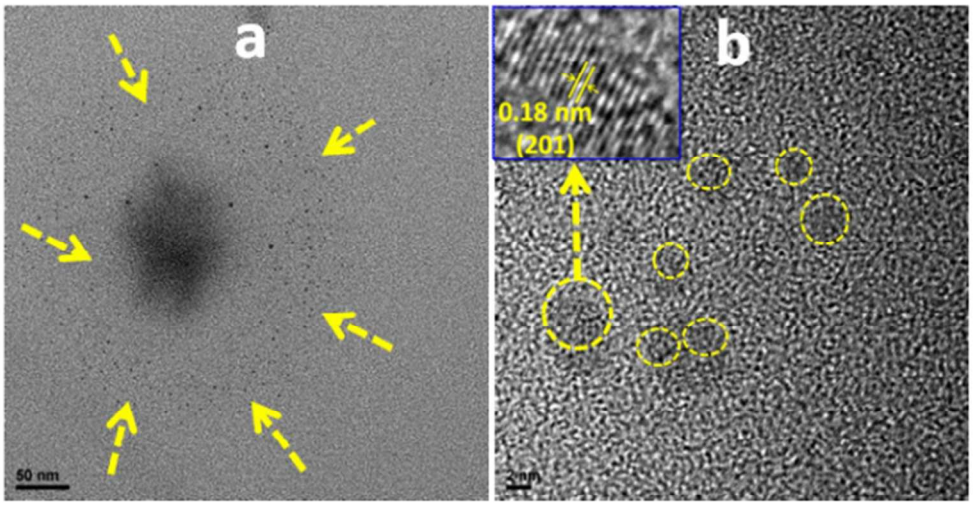

Fig.4

Apurav *et al.*

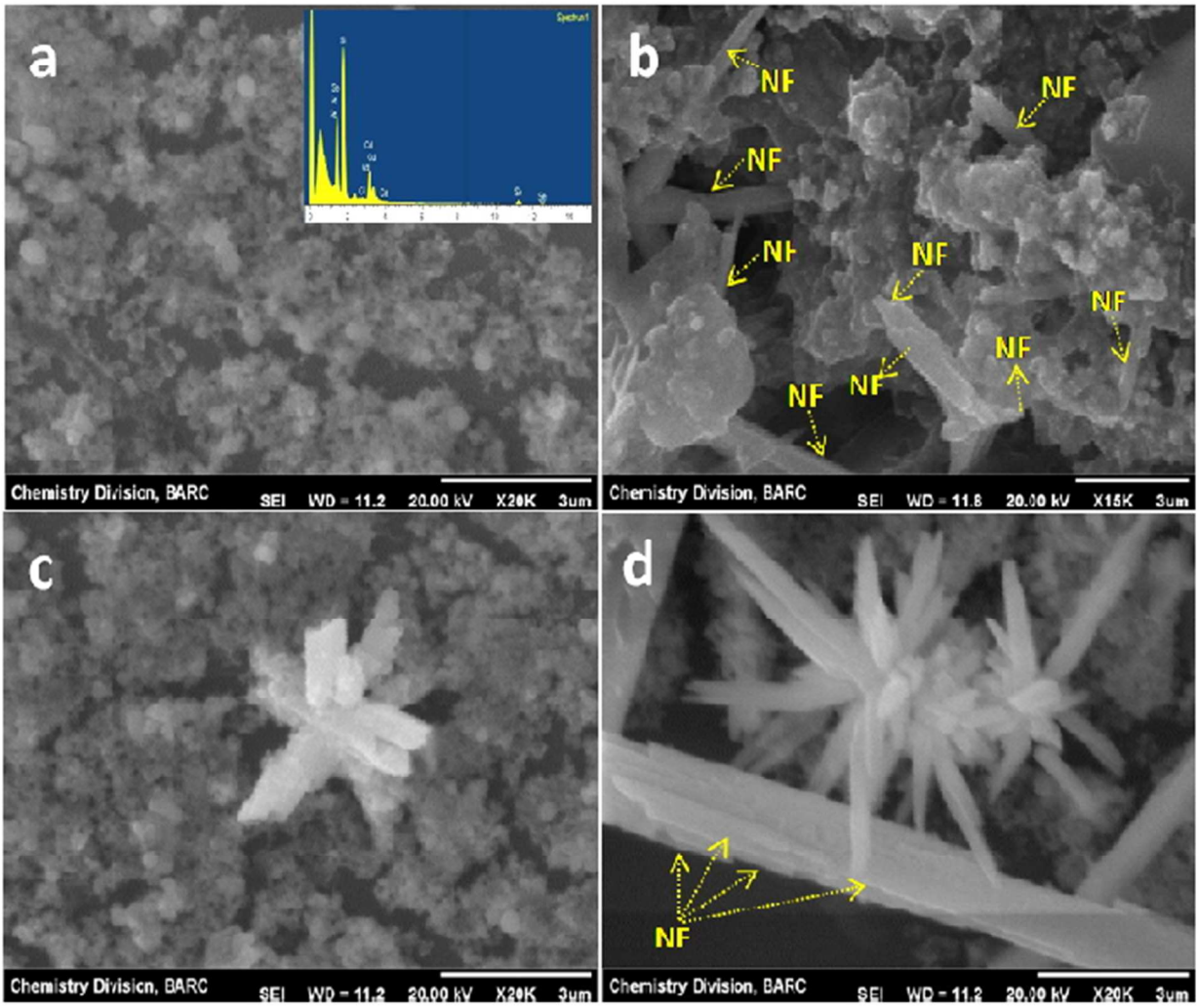

Fig.5

Apurav *et al.*

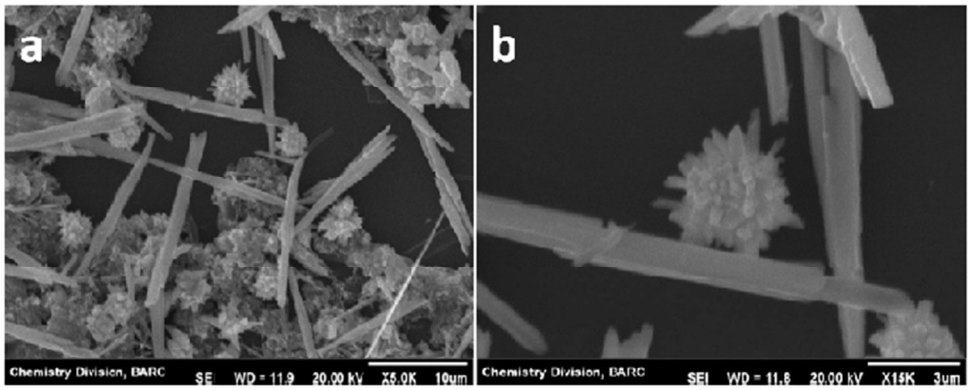

Fig.6

Apurav *et al.*

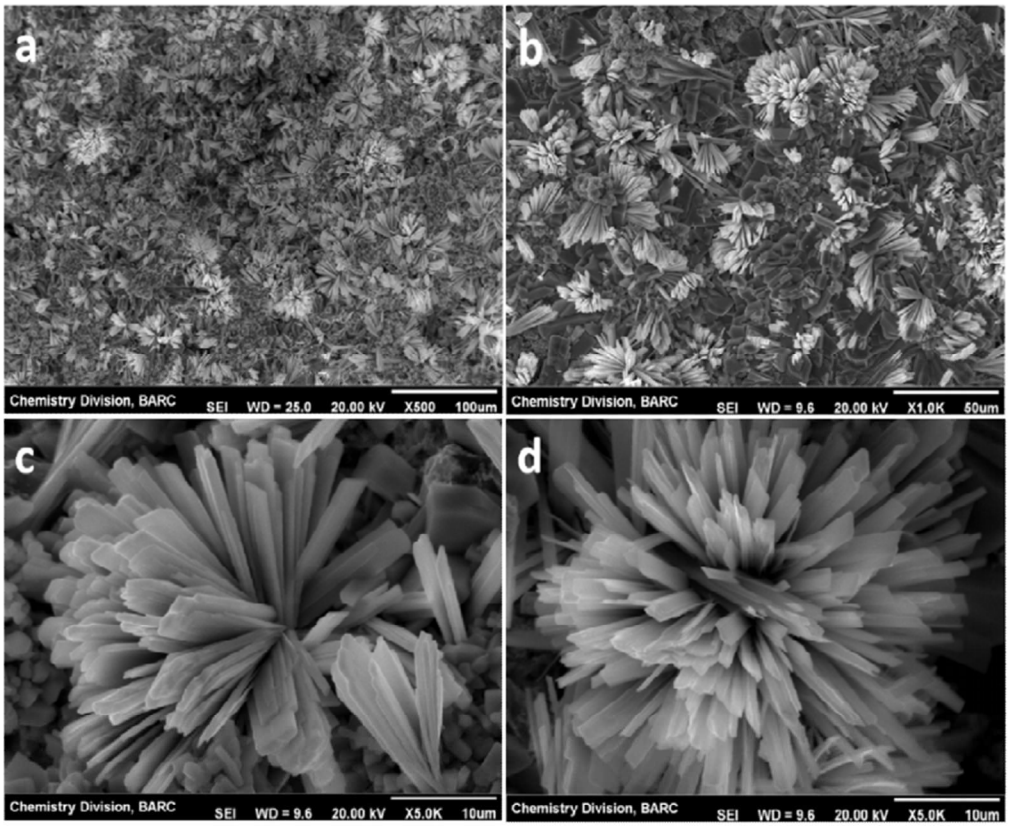

Fig.7

Apurav *et al.*

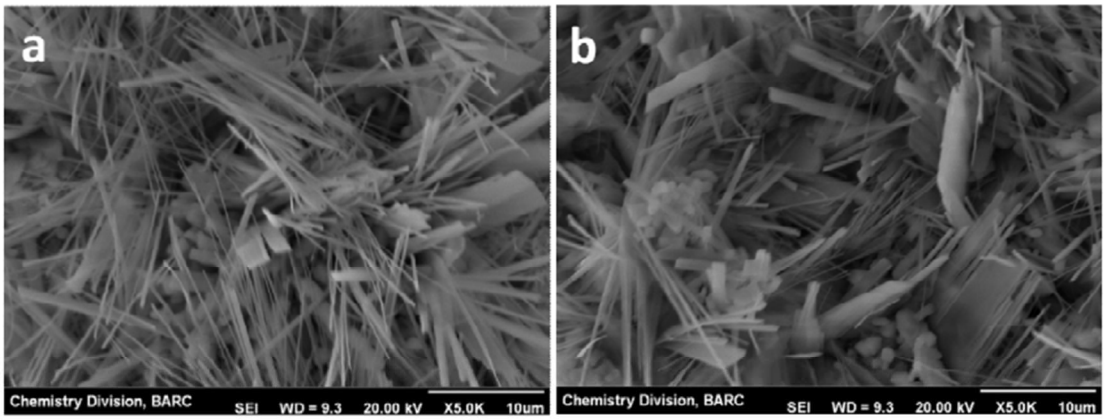

Fig.8

Apurav *et al.*

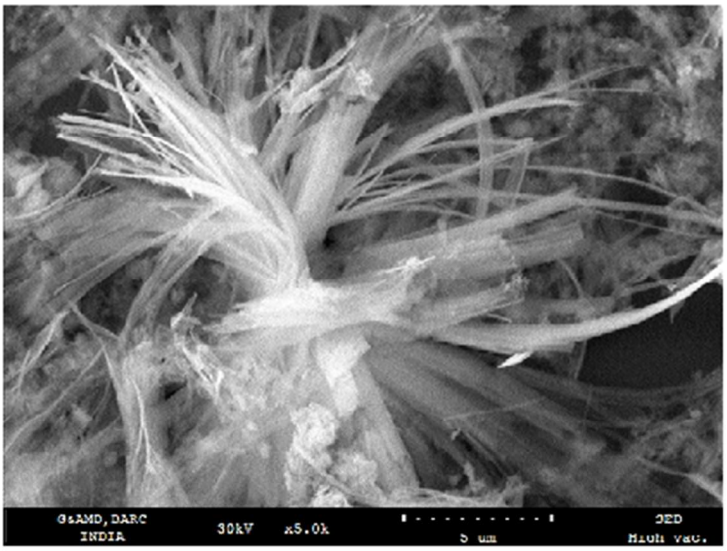

Fig.9

Apurav *et al.*

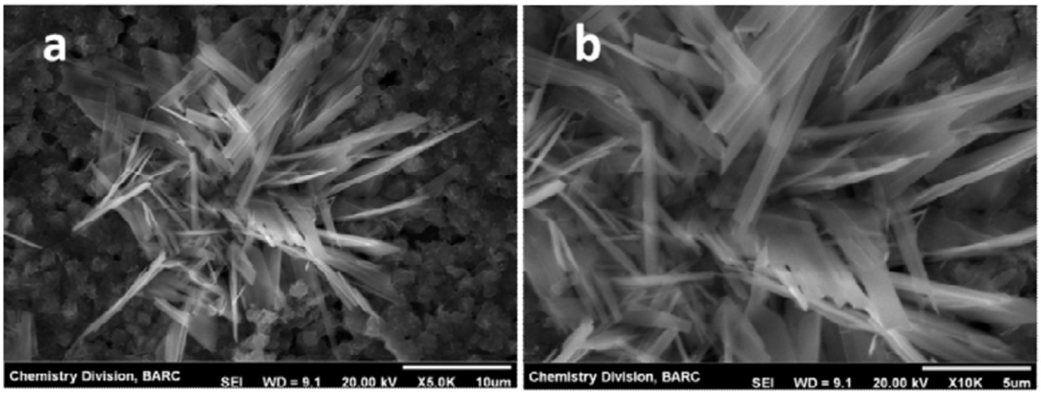

Fig.10

Apurav *et al.*

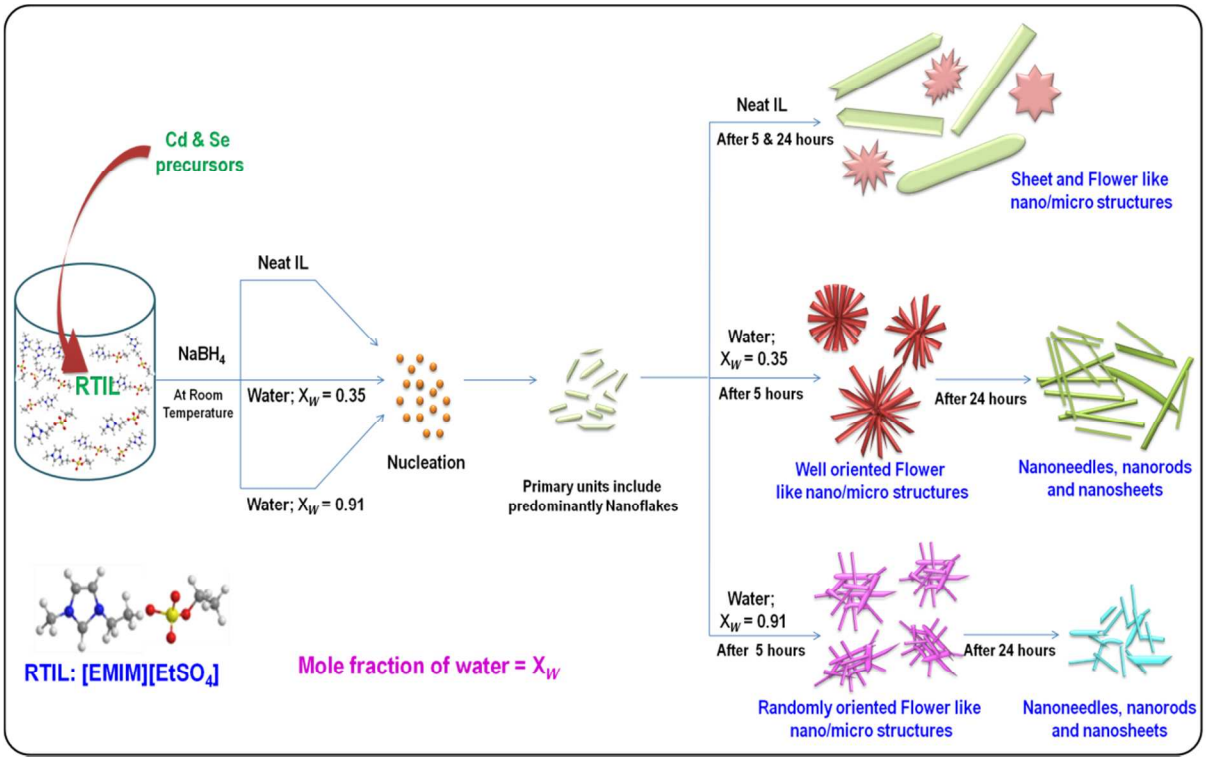

Fig.11

Apurav *et al.*

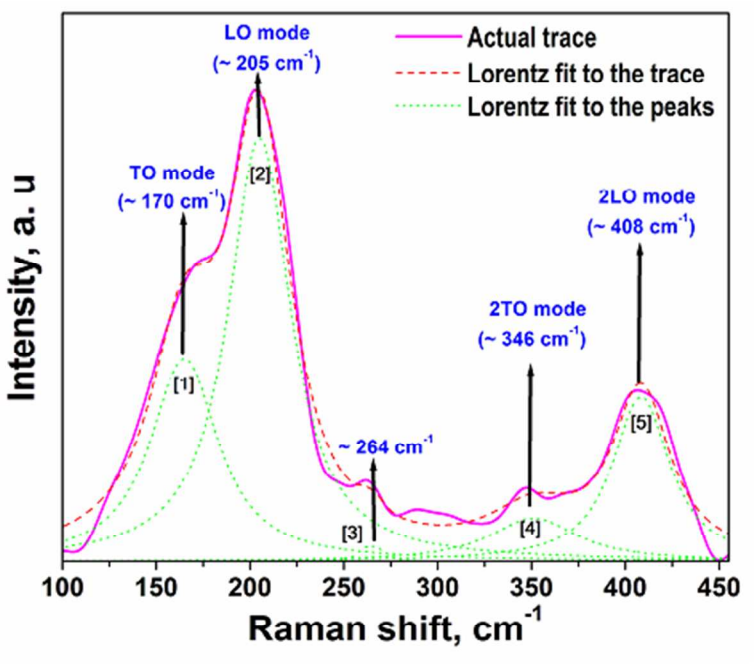

Fig.12

Apurav *et al.*

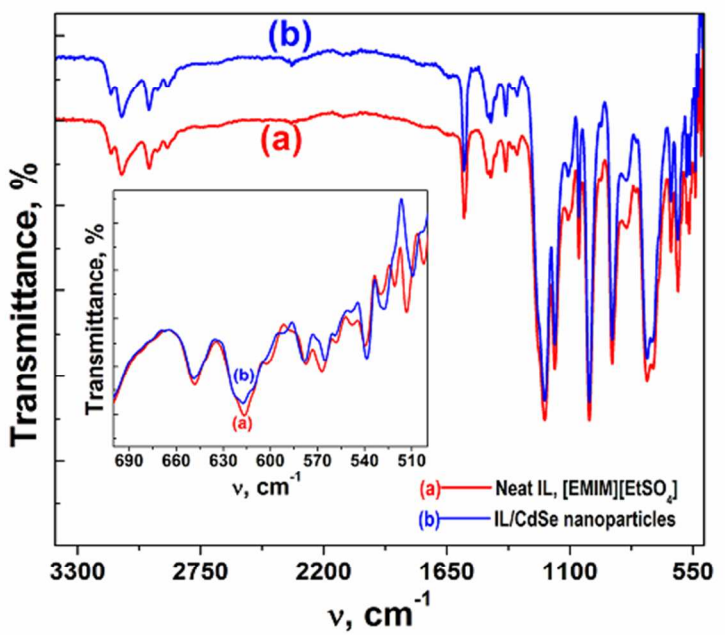

Fig.13

Apurav *et al.*

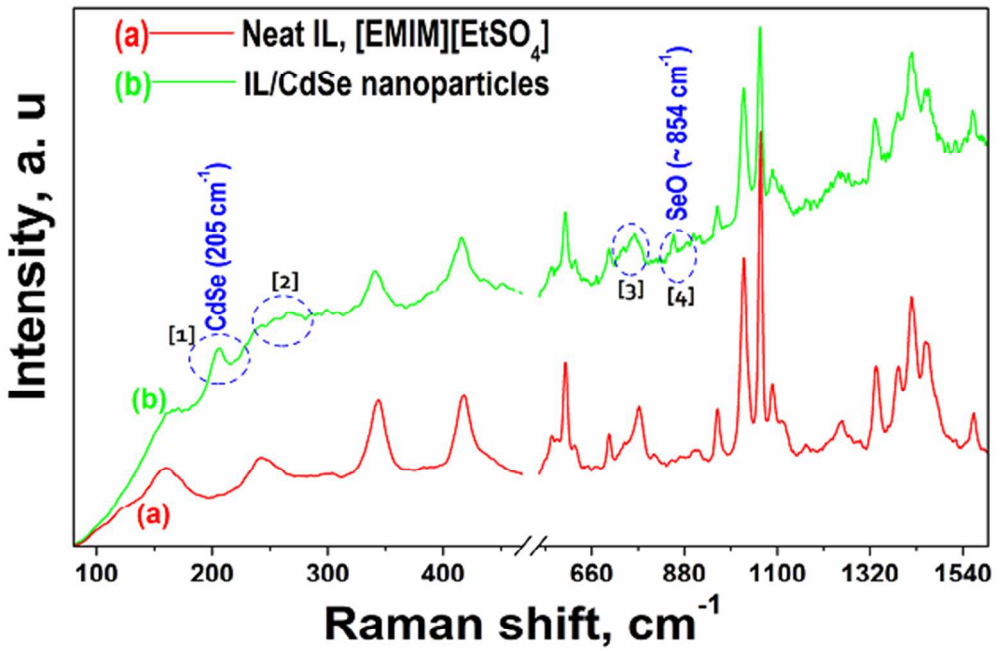

Fig.14

Apurav *et al.*

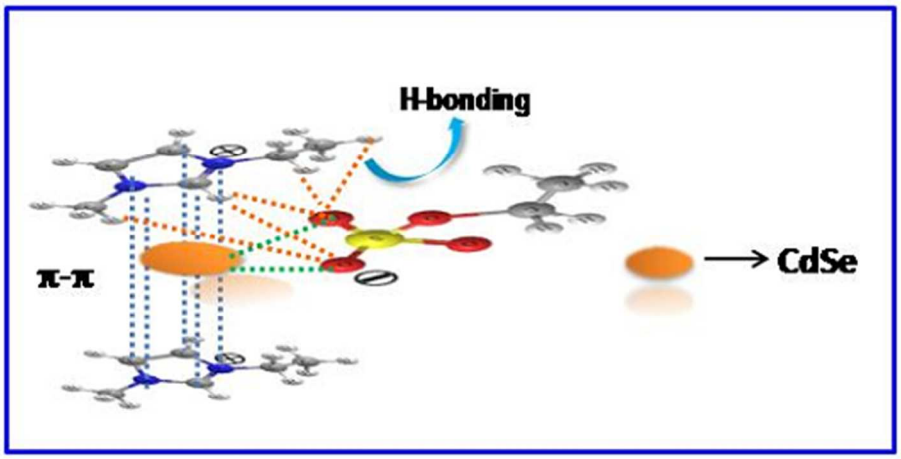

Fig.15

Apurav *et al.*

Table of Contents Graphic

Role of structural and fluidic aspects of Room temperature ionic liquid in influencing the morphology of CdSe nano/microstructures grown *in situ*

Apurav Guleria, Ajay K Singh, Madhab C Rath, Sisir K Sarkar and Soumyakanti Adhikari*

Radiation & Photochemistry Division, Bhabha Atomic Research Centre, Mumbai 400 085, India

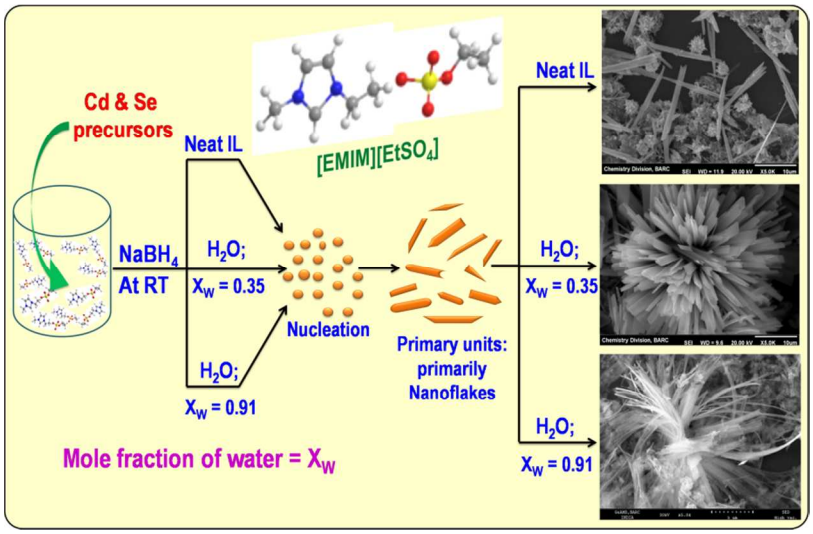

CdSe nanoparticles were synthesized in *neat* imidazolium IL to examine the influence of intrinsic structure of RTIL on their nanomorphology. Herein, RTIL played multiple roles i.e. solvent, stabilizer and shape directing template.